ESD Experiment Results on Ground Using Experiment Model of HORYU-IV

Hiroshi Fukuda[*]
Laboratory of Spacecraft Environmental Interaction Engineering, Kyushu Institute of Technology, Tobata, Kitakyushu, 804-8550, Japan

Tatsuo Shimizu[†]
Reaktor Space Lab Oy, Otakaari 5, Espoo, 02150, Finland

Kazuhiro Toyoda[‡] and Mengu Cho[§]
Laboratory of Spacecraft Environmental Interaction Engineering, Kyushu Institute of Technology, Tobata, Kitakyushu, 804-8550, Japan

HORYU-IV is a 30 cm cubic satellite with an approximate mass of 11 kg. The satellite was successfully launched by a JAXA H-IIA rocket to an orbit of 575 km altitude with a 31º inclination on February 17, 2016. HORYU-IV's main mission is to capture an Electro-Static Discharge (ESD) current waveform by an onboard oscilloscope and capture its image by a camera triggered by the oscilloscope. HORYU-IV captured various ESD current waveforms and images in space. Ground-based experiments were carried out to compare the waveforms between the flight results and the ground results. The results of ground-based experiments, compared with the flight results, had lower peak currents and longer durations. This result does not match past ground-based experiments showing that ESD current has lower peaks and longer durations when ambient pressure is lower. Also, we found the relationship between ESD occurrence location and ESD current waveforms through ground-based experiment.

[*] Postgraduate Student, Department of Electrical and Electronic Engineering, Laboratory of Spacecraft Environment Interaction Engineering, 1-1 Sensui Tobata, Kitakyushu.
[†] Chief Scientist, Reaktor Space Lab Oy, Otakaari 5, Espoo, Finland, Senior Member AIAA.
[‡] Associate Professor, Laboratory of Spacecraft Environment Interaction Engineering, 1-1 Sensui Tobata, Kitakyushu. Senior Member AIAA.
[§] Professor, Laboratory of Spacecraft Environment Interaction Engineering, 1-1 Sensui Tobata, Kitakyushu. Senior Member AIAA.

I. Introduction

WHEN a spacecraft power system needs to provide high power, higher solar array voltage has advantages such as improvement of transmission efficiency and reduction of cable mass. When we consider a simple circuit of power supply system, the power loss of transmission cable is described by following equation.

$$\frac{\Delta P}{P} = P\frac{\rho l}{SV^2}$$

Here ΔP is the power loss of transmission cable, P is generating power, ρ is the resistivity of transmission cables, l is the length of cables, S is the cross section of cables, and V is the transmission voltage. This equation shows that the power loss of transmission cable is inverse proportion to the transmission voltage. Also, the larger generating power leads the larger power loss of transmission cable if we don't do anything. In order not to increase the power loss of cable, there are several methods. The one of them is increase the cross section of transmission cable. This method leads the increases of transmission cable mass. Another is increasing the transmission voltage. The high voltage transmission is advantageous to reduce the power loss. However, high voltage operation in space has a high risk of electrostatic discharge (ESD) [1, 2]. Higher solar array voltage raises the risk of getting ESDs due to the spacecraft charging caused from interaction with ambient plasma. Typically, the spacecraft ground is connected to the negative end of a solar array. When a negative grounded solar array generates power in Low Earth Orbit (LEO), most of spacecraft surface has negative potential with respect to the ambient plasma due to the thermal velocity differences between electrons and ions. ~~and it has negative potential which is equivalent to generating voltage in a Low Earth Orbit (LEO).~~ On the other hand, the spacecraft surface insulator has a relatively positive potential almost equal to its plasma potential (Fig. 1). Once the potential difference between the surface insulator and the solar array conductor exceeds a threshold value, an ESD may occur at a triple junction point (i.e., contact points of conductor, insulator, and vacuum). ESD on the solar array can lead to damage on solar array and even can cause the loss of the satellite. According to Ref. [1], -200 V is a threshold voltage of ESD and 160 V operation on the International Space Station is the highest solar array voltage used in orbit. However, future space missions may need a mega-watt order of power. For these missions, high voltage technology in space is indispensable. In order to avoid failure due to ESDs and establish high voltage technology, it is necessary to study the mitigation of ESD on a solar array through ground-based testing and computer simulations. The one of the ESD mitigation method is covering all exposed electrode. Because of the area which mounted solar cells is huge, it is not realistic method to adapt to high power spacecraft.

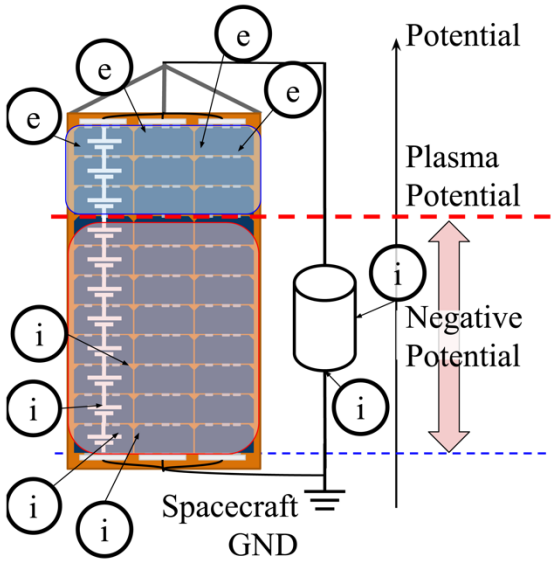

Fig. 1 Schematic of spacecraft potential with negative grounded solar array in LEO.

In order to achieve high voltages in space, various experiments have been conducted. However, it is difficult to simulate a complex space environment with variables such as spacecraft motion, vacuum pressure, and plasma conditions. Therefore, an experiment in such an environment has not been conducted on a ground-based system. In addition, it cannot be concluded that the ESDs observed on the ground are exactly the same as those in a real space environment.

To evaluate the validity of ground-based experiment results, several payloads were launched. HORYU-II is a 30 cm cubic satellite which has been developed and operated by the Kyushu Institute of Technology (Kyutech). This satellite was launched in May 2012 and put into a 680 km, 98.2º sun-synchronous orbit. The main mission of this satellite is high voltage (347 V) generation in a real space environment [3]. HORYU-II succeeded in generating 347 V continuously in orbit and that high voltage was used for ESD experiments as a bias source [4, 5]. From the ESD experiments, HORYU-II successfully detected several ESDs on a solar array. However, unexpected ESDs were observed on an ESD mitigated solar array. HORYU-II was designed only for ESD detection and could not determine where these ESDs occurred and how the ESD current flowed.

Therefore, HORYU-IV, which is a successor to HORYU-II, was launched on the 17th of February 2016 by a H-IIA rocket into a 575 km, 31º circular orbit. The major update from HORYU-II to HORYU-IV was to add an in-house developed oscilloscope and to add a camera to capture images. The intent is to measure ESD currents and get images with the same quality as ground-based experimental systems. The data was used for comparing the ESD experiment

results. We conducted an ESD experiment after one week from the launch and successfully measured the ESD current and captured images as reported in Ref. [6, 7]. From the initial operation, we could confirm that in-house developed instruments for ESD measurement worked. This paper presents the results of ground-based ESD experiment using the experiment model of HORYU-IV. We also compare the flight results with ground-based experiment results.

This paper includes four parts. The second part describes the satellite overview and the ESD experiment system. The third part describes the ground-based ESD experiment results which used an experiment model of HORYU-IV. The experiment was carried out in a vacuum chamber equipped with an ECR plasma source. Finally, the fourth part is the conclusion and suggests future research.

II. Satellite Overview and ESD Experiment System

Table 1 shows the specifications, and Fig. 2 shows the exterior of HORYU-IV. This satellite does not have any active attitude control system. Instead, it is equipped with a permanent magnet for field-aligned control around the X axis. This satellite has three different types of solar array: bus solar array for satellite operation, high-voltage solar array (HVSA) as a bias source of ESD experiment, and solar array coupons for the ESD experiments. The solar array coupons for ESD experiment are mounted on the +Z and -Z panel. As a feature of this satellite, the -Z side has a 7 cm arm equipped with a convex mirror at the tip. The +Z panel has a hood structure and the area for mounting solar array coupons is recessed to about 12 cm on the satellite's inner side.

Table 1 Specifications of HORYU-IV

Size	30 × 30 × 30 cm
Mass	11 kg
Power	Triple junction 34 cells in total (avg. 1 W/Cell) Ni-MH Battery (5700 mAh)
Attitude Control	Field-aligned control by permanent magnet (Alnico5, Surface magnetic flux density: 150 mT)
Communication	UHF/VHF 1.2 kbps, S-band 100 kbps
Launch	17th February 2016, H-IIA rocket
Orbit	575 km, 31 deg

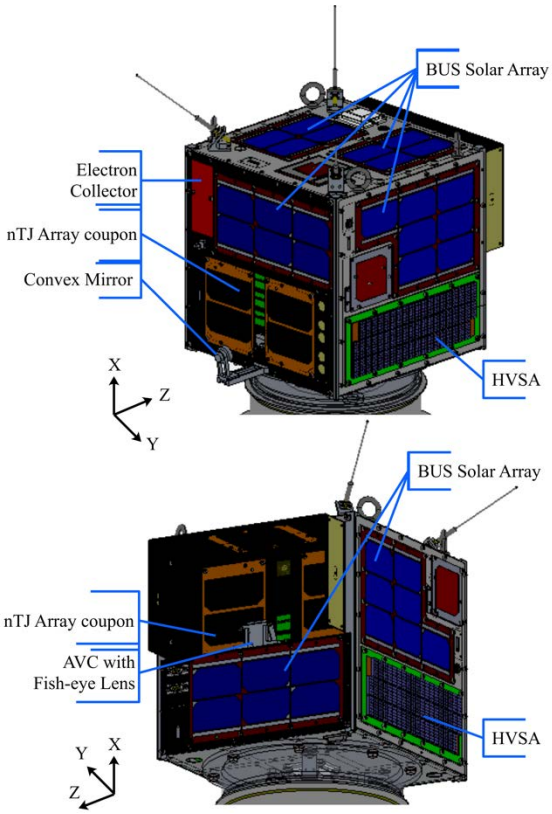

Fig. 2 Exterior of HORYU-IV.

As a bias source of ESD experiment, the HVSA is mounted. This HVSA is composed of 58 pieces of Sphelar Array® which is about 24 mm × 9.5 mm, and is able to generate up to 420 V. In the ESD experiment, this voltage is clamped to 347 V by a Zener diode (three DZF27C100P and one SML4756). As indicated previously, this satellite rotates around the X axis at about 2 degree/sec. Therefore, HVSAs are mounted to face each other and connect in a series the HVSAs have bypass diode to be able to generate high voltage regardless of attitude. Furthermore, in order to prevent any ESD on the HVSAs, all exposed electrodes are covered with silicone adhesive.

The solar array coupons for the ESD experiment are mounted on the satellite panel. All of the ESD experiment coupons are made of two series connected 8 cm × 4 cm GaAs/InGaP/Ge (3G30A, AZUR SPACE). The nominal type triple junction solar array coupon (named nTJ Array coupon) (shown in Fig. 3) has solar cells attached to an aluminum substrate covered with Kapton tape. The substrate of nominal type coupons, which is mounted on the +Z panel, is also biased when the ESD experiment is executed on this coupon. The substrate of the -Z panel nominal type coupon floats electrically.

- ~~Nominal type Triple Junction Solar Array coupon (nTJ Array coupon) (Shown in Fig. 2)~~

~~The nominal type coupon has solar cells attached to an aluminum substrate covered with Kapton tape. These are mounted on the +Z and -Z panel. The substrate of nominal type coupons, which is mounted on the +Z panel, is also biased when the ESD experiment is executed on this coupon. The substrate of the -Z panel nominal type coupon floats electrically.~~

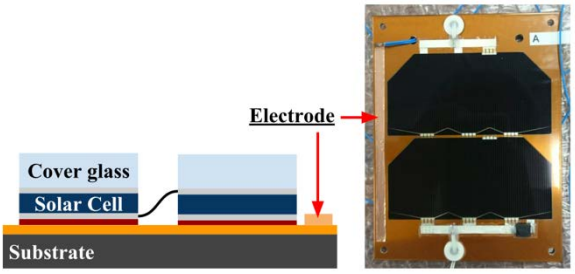

Fig. 3 Basic principle of nTJ Array coupon.

Figure. 4 shows a configuration of an ESD experimental system. Electron collectors are used so that the experimental system ground has a highly negative potential against the ambient plasma potential. During the experiment, the solar array coupon is connected to HVSA. When an ESD occurs, electric charge stored in an external capacitor which written "C_{EXT} 0.1μF" in the Fig. 4 is released. The total ~~ESD capacitance~~ electric charge released by an ESD is about 34.7 μC calculated by biasing voltage multiplied by external capacitance. The solar array coupons, as shown in the image from Fig. 3, have an electrode made of copper tape and have the same potential with the electron collector and work as an anode spot of ESD events. The distance between the edge of a solar cell and an anode electrode is 1 mm.

The in-house developed on-board oscilloscope (OBO) is used for measurement of ESD currents. These ESD currents are converted into voltage using current transformers, and are recorded with a sample speed of 6 or 40 MHz. The measurement dynamic range is -10.2 to +71.7 A with an 8-bit resolution (i.e. the OBO system can measure a 0.32 A step). The OBO system has two types of measurement mode, single-channel mode and multi-channel mode. In the single-channel mode, the OBO measures only CH1, which is located under the electron collector, as shown in Fig. 4. In the multi-channel mode, the OBO measures CH1, CH2, and CH4 during nTJ array testing. The trigger level is adjustable at all ranges with irregular steps, for example from 2 to 20 A in 2 A steps, and from 20 to 25 A in 1 A steps, changeable by uplink commands from the ground station.

Two Arc Vision Cameras (AVCs) are mounted on the +Z and -Z side. The camera of the +Z is equipped with a fisheye lens, it can shoot at a wide angle. The opposite side has a convex mirror which can reflect the entire -Z surface

so that by shooting this mirror, it can take an image of the -Z side from inside the satellite. The video signal is fed into the capture board to record video frames which include before and after each ESD. The AVC can save 2.8 frames in one shot and can store up to 24 events. AVC shutter timing is synchronized with an OBO trigger signal which is sent when an ESD is detected in the OBO.

The ESD experiment system except for the OBO and the AVC is isolated from the satellite bus system to avoid any affect to the bus system. The ESD experiment has its own system ground which has a highly negative potential when generating high voltage compared with ambient plasma. On the other hand, the ESD measurement system uses a satellite bus ground. The details of the OBO and AVC system are described in Ref. [8].

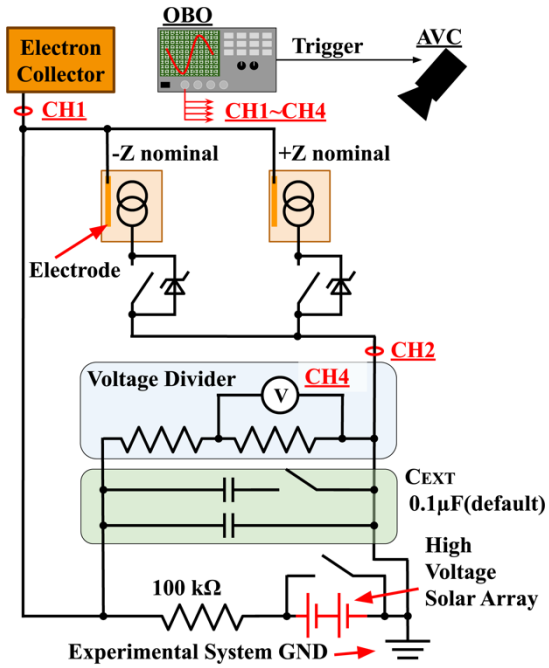

Fig. 4 ESD experiment system configuration.

III.Ground-based ESD Experiment Results

Figure. 5 and Fig. 6 are flight results of the ESD current waveform and images which were reported in Ref. [7]. As can be seen from Fig. 5, the waveform has an about 60 A of peak current and about 1 μs duration. From the captured images of spark light from ESD as shown in Fig. 6, the faint spark light is recorded at the front with an arrow. This ESD occurred at the edge of the solar cell which was close to the anode electrode. Several other ESD current waveforms have been reported, and most of the waveforms have 50 to 60 A of peak current and about a 1 to 1.3 μs duration. Furthermore, these ESDs occurred in similar locations which were close to the anode electrode.

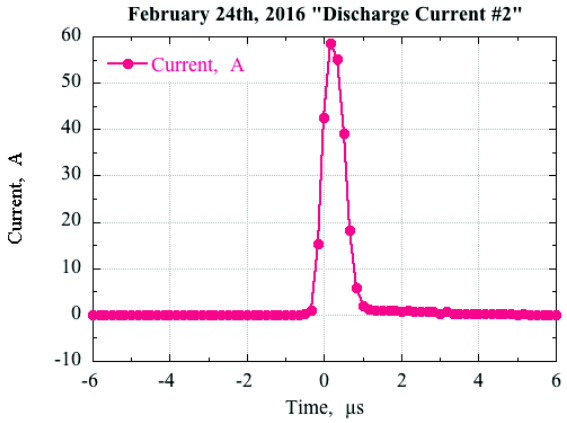

Fig. 5 ESD current waveform recorded in OBO through flight experiments. [7]

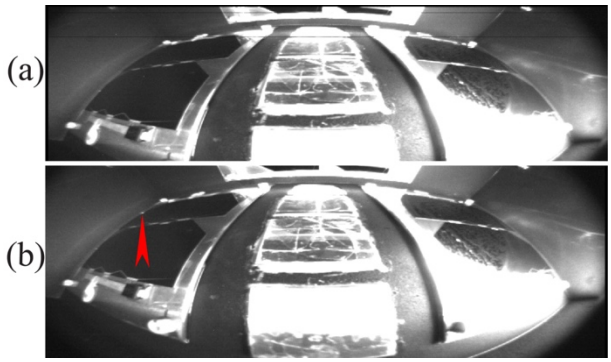

Fig. 6 ESD image recorded in AVC through flight experiments. [7]

(a) Recorded image before ESD occurred
(b) Spark light from ESD is at the front with an arrow

A. Ground-based ESD Experiment #1

In order to compare the flight results with those measured in the ground-based experiment, we performed ESD experiment with the experiment model of HORYU-IV. The experiment configuration is shown in Fig. 7. The experiment was carried out 100 minutes on the +Z side nominal-type coupon using a stainless-steel vacuum chamber (1.0 m diameter, 1.2 m length). A Xenon plasma with an electron density of 2.6×10^{11} m^{-3}, electron temperature of 2.3 eV, and pressure of 2.0×10^{-3} Pa environment was generated by an ECR plasma source. The plasma parameter was measured by a 3.0 cm spherical Langmuir probe. This electron temperature is one order of magnitude higher than the temperature in orbit. It is not possible for the plasma source to reproduce the same plasma parameters as those in the flight condition. The circuit configuration was the same as the flight experiment shown in Fig. 4. The satellite bus power was supplied by a DC power supply outside of the vacuum chamber. The high voltage was generated by HVSA, which was illuminated by a halogen lamp from outside of the chamber. The satellite bus system's electrical ground was connected to the vacuum chamber. The ESD experiment system used its own circuit ground (named high voltage system GND) which was highly negative with respect to the plasma potential. All measurement data such as ESD current data and image data were sent via the S-band downlink. Following this, the data was received at the ground station of Kyutech. During the 100 minutes of the ESD experiment, 10 ESDs were detected so that the ESD rate was 0.10 times per minute. Based on ESD current waveforms, the ESD events were categorized into three ~~types~~, ~~The ESD current type-A has~~ a higher range (more than 40 A) peak current, ~~the type-B has~~ a middle range (between 15 A and 40 A), and ~~the type-C has~~ a lower range (lower than 15 A). Table 2 shows the timing of ESD detection, the type of

ESD current waveform, peak current and duration of each ESD. The duration is defined as the interval from rise to fall of 5% of peak current.

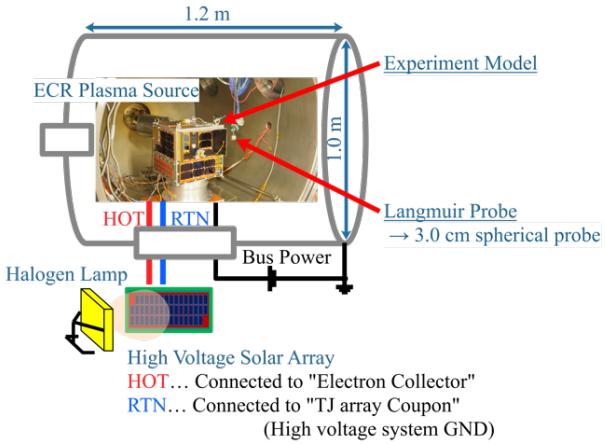

Fig. 7 Configuration of Ground-based ESD Experiment #1.

Table 2 Summary of the ESD experiment on ground [+Z nominal Single channel mode].

ESD number	ESD timing, sec	~~ESD current type~~	Peak current, A	Duration, μs	Electric charge, μC
#1	952	~~B~~	25.0	2.0	23.7
#2	1,037	~~B~~	18.2	2.3	20.7
#3	1,066	~~B~~	19.8	2.3	21.2
#4	1,242	~~C~~	12.5	4.7	18.9
#5	1,302	~~B~~	17.6	2.5	20.6
#6	1,431	~~B~~	18.6	2.3	20.4
#7	2,141	~~B~~	16.3	2.7	19.4
#8	3,049	~~A~~	45.1	1.3	33.6
#9	3,588	~~A~~	45.8	1.3	34.0
#10	5,817	~~B~~	16.4	3.0	19.1

Figure. 8, 10 and 12 show the ESD current waveforms of ESD number #2, #4, and #9, respectively. The electric charge calculated ~~of electric charges~~ from the ESD current waveform was 23.7 μC, 18.9 μC, and 34.0 μC, respectively. These values were 68.3%, 54.5% and 98.0% compared to the theoretical value, respectively. There is relationship between the peak current and the electric charge released by ESDs. Figure. 9, 11 and 13 show the ESD images of those. At the tip of the arrow, there is a faint spark light emission of the ESD. ~~The order of video frames is from the bottom to the top (i.e., the bottom image (frame 1) is the earliest and the top image (frame 3) is the latest).~~ The AVC was operating in interlace-video mode with the frame rate of 120 Hz. ESD number #9 is the most similar to the flight data which was shown in Fig. 5. Both ESD occurrence locations were the edge of the solar cell and were located at about a 1 mm distant from the electrode. The flight data, however, has a shorter duration and a higher peak current compared with the ground results. According to Ref. [9], the ESD current peak tends to become higher when the

ambient pressure is high. The observation on the ground test does not match the flight data. Figure. 14 shows the relationship between the peak current and the distance between the ESD location and anode electrode. Some AVC images had noise and we could not identify the location of the ESD; therefore, Fig. 14 was created using other clearer images. As can be seen from this graph, the peak value of the ESD current has a correlation with distance between the electrode on the coupons and the ESD location. The shorter the distance between the ESD location and the anode electrode, the higher the peak current and the shorter the pulse width became. This may be due to the plasma resistance being smaller for a shorter distance. Moreover, the ESD current waveform becomes a gentle slope with a slow rise in the current as the ESD location is farther from the anode electrode.

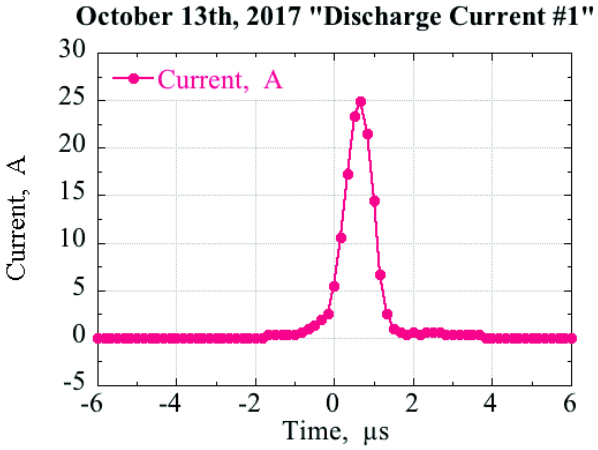

Fig. 8 ESD current waveform of ESD #2 (~~ESD Type B~~ middle range).

Fig. 9 AVC image of ESD #2 (~~ESD Type B~~ middle range). [Superimposed image]

(a) Recorded image before ESD occurred
(b) Spark light from ESD is at the front with an arrow

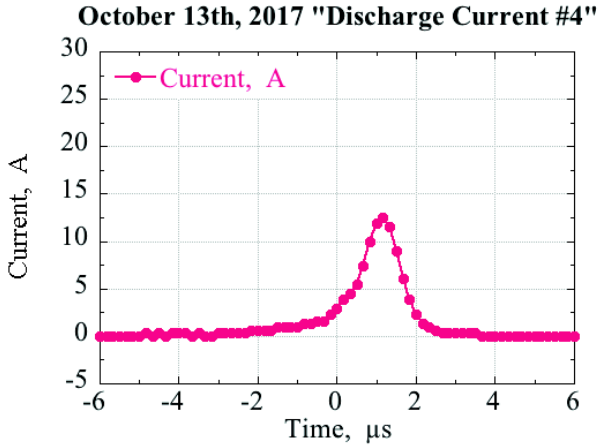

Fig. 10 ESD current waveform of ESD #4 (~~ESD Type C~~ lower range).

Fig. 11 AVC image of ESD #4 (~~ESD Type C~~ lower range). [Superimposed image]

(a) Recorded image before ESD occurred
(b) Spark light from ESD is at the front with an arrow

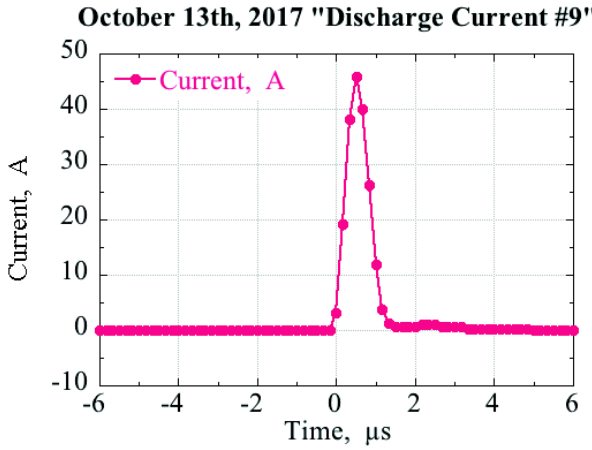

Fig. 12 ESD current waveform of ESD #9 (~~ESD Type-A~~ higher range).

Fig. 13 AVC image of ESD #9 (~~ESD Type-A~~ higher range). [Superimposed image]

(a) Recorded image before ESD occurred
(b) Spark light from ESD is at the front with an arrow

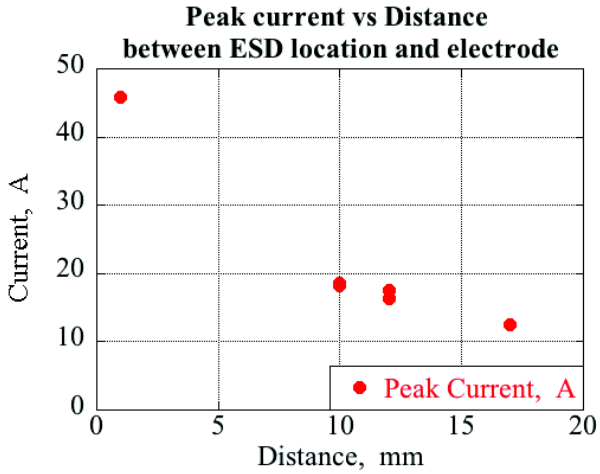

Fig. 14 Peak current vs. Distance between ESD location and electrode.

B. Ground-based ESD Experiment #2

What we found thorough Ground-based ESD Experiment #1 is that the ESD current waveforms vary depending on the distance between ESD location and anode electrode. However, we could not confirm the ESDs further than 17 mm from anode electrode. Therefore, we conducted further ESD experiments to confirm the behavior of ESD current waveforms. Figure. 15 shows that the configuration of Ground-based ESD Experiment #2.

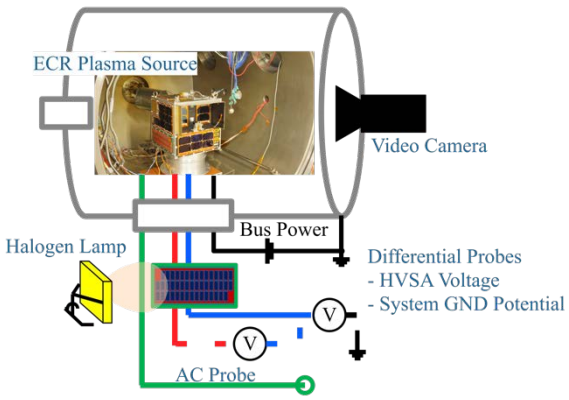

Fig. 15 Configuration of Ground-based ESD Experiment #2.

In addition to the configuration of ESD Experiment #1, a differential probe (Pico Technology, TA044) and an AC probe (Tektronix, P6022) were installed. The differential probe was used to measure the potential of high voltage system GND and the voltage of HVSA. Additionally, the AC probe was used to measure an ESD current waveform so that the AC probe could be installed to the ESD current route which was located inside the satellite. In order to take a picture of the spark of light from the ESD, a video camera was installed outside the chamber. In this experiment, the following two measurement systems were adopted.

- Measurement system 1: On-board measurement system (OBO and AVC)
- Measurement system 2: Ground equipment (National Instruments, PCI-5105 and in-house video capture system called Quick Look system)

As in ESD Experiment #1, a Xenon plasma with an electron density of 2.7×10^{11} m^{-3}, electron temperature of 2.3 eV, and pressure of 2.0×10^{-3} Pa environment was generated by an ECR plasma source. In the total five hours of biased time, 10 ESDs were detected on measurement system 2, on the other hand, only one ESD was detected on measurement system 1. Here, we focus on the ESDs (named group-1) which were not detected on measurement system 1. Figure. 16 shows the ESD current waveform which has the highest peak current in group-1. The potential of high voltage system GND is also shown in Fig. 16.

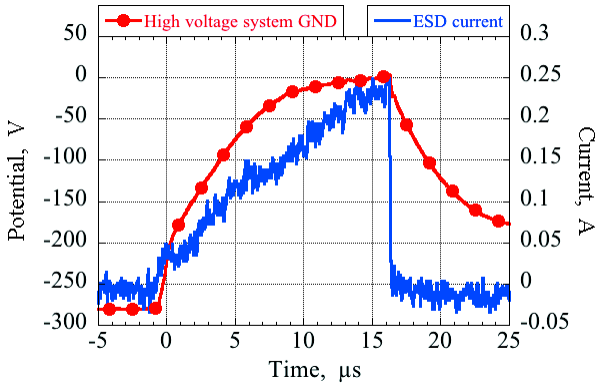

Fig. 16 Measurement data of Ground-based ESD Experiment #2.
(Red: Potential of high voltage system GND) (Blue: ESD Current)

Before this ESD occurred, the high voltage system GND potential had around -280 V, as shown in Fig. 16. The cover-glass had almost the same potential as the ambient plasma, and the electrode had a slightly high potential compared with the ambient plasma. Once this ESD occur, the high voltage system GND potential rose to around 0 V. The distribution of potential of high voltage system GND is the trend of blow-off capacitance (which high voltage system has capacitance respect to the ambient plasma). When ESD occur, blow-off capacitance is released to the ambient plasma. The ambient plasma has resistance so that the discharge path is functioning like a RC circuit. When ESD finished, the blow-off capacitance charged again due to plasma interaction. Therefore, it is considered that the potential of high voltage system GND traced the shark-fin shape. Moreover, the anode electrode potential rises corresponding to the high voltage system GND potential. When the potential of the high voltage system GND reaches around 0 V, the ESD current also reaches a peak current. ~~Then, the experiment coupon charged again due to plasma interaction.~~ The electric charge calculated from the ESD current waveform was 2.37 µC. This value was equivalent to just about 6.8 % of electric charges which were stored in C_{EXT}. During the process of high voltage system GND potential rising, the capacitance, which the experiment system had, also discharged and released a blow-off current. Therefore, not all of the electric charges (2.37 µC) were discharged from the C_{EXT}. Figure. 17 shows the ESD location. The ~~above~~ ESD shown in Fig. 16 occurred at the 20 mm distant from anode electrode around the interconnector between the two cells. The other marks indicate the other nine ESDs occurrence locations of group-1.

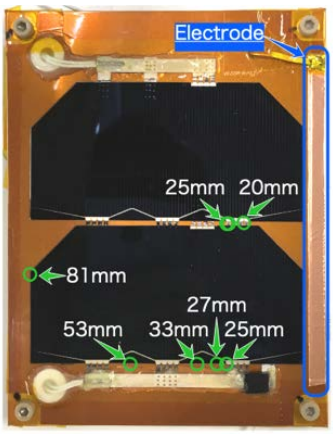

Fig. 17 ESD locations of group-1.
(The numbers are distances between the anode electrode and ESD location)

Figure. 18 shows the relationship between a peak value of ESD current and an ESD location. The red dot shows the results of ESD Experiment #1, and the blue dot shows that of ESD Experiment #2. As shown in this figure, the peak value of ESD current decreases as the distance between the ESD location and the electrode increases. Here, we discuss the electric field around the experiment coupon. Figure. 19 shows the schematic drawing of an electric field formation around the experiment coupon. Usually, the electrons emitted from ESD location travel to the point which has a higher potential while following the electric field. It is considered that when the ESD occurs at a location far from the anode electrode as in CASE-1 in Fig. 19, the electric field around the ESD location is formed in the direction of the ESD location from the sheath boundary. Therefore, the emitted electrons travel to the sheath boundary while colliding to the neutral particles, which then travels to the anode electrode. Because of long ESD current path, however, the ambient plasma resistance may be high enough to cut-off the ESD, and the capacitance stored in C_{EXT} cannot be completely discharged. As a result, it is considered that the peak value of ESD current becomes small and ESD current falls rapidly. On the other hand, it is considered that when the ESD occurs at a location close from the anode electrode, as in CASE-2 in Fig. 19, the electric field is formed in the direction of the ESD location from the anode electrode. Therefore, the emitted electrons travel to the anode electrode directly. Since the path through which the emitted electrons travel is short, the plasma resistance is considered to be small. As described in Fig. 18, when the distance between the anode electrode and the ESD location is about 20 mm or more, the peak value of ESD current abruptly decreased. We did not observe these ESDs through flight experiment or through ESD Experiment #1. This is because the trigger level was set at 4 A in the OBO system and the experiments were conducted. Therefore, a small ESD, such

as the results of ESD Experiment #2, are not possible to detect on-board satellites. This means that there was a possibility that more ESD occurred in the flight experiments.

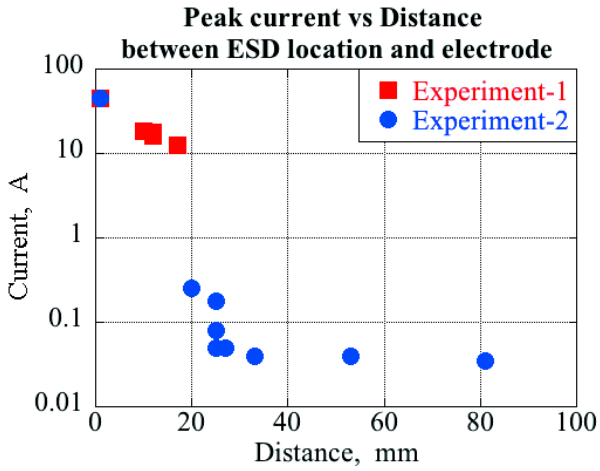

Fig. 18 Peak current vs. Distance between ESD location and electrode.
(Red: Experiment #1) (Blue: Experiment #2)

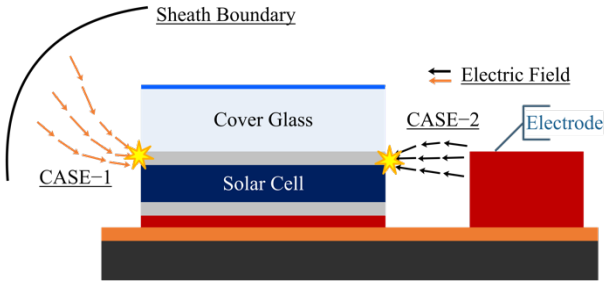

Fig. 19 Electric field formation at edge of solar cell.

IV. Conclusion

A ground-based ESD experiment was carried out using an experiment model of HORYU-IV. The experiment coupons made of two series connected 8 cm * 4 cm GaAs/InGaP/Ge solar cells. In addition to the conventional design of solar array layout, electrodes which worked as an anode spot of ESD were mounted just beside the solar cells. The experiment model of HORYU-IV was put inside a vacuum chamber, and high voltage and bus voltage were supplied from outside of the chamber. Through 100 minutes of experiment under LEO simulated plasma environment, 10 ESDs were detected. The shapes of ESD current waveforms captured in ground-based experiment and flight experiment were similar. However, the ESD current of flight data had a higher peak current and shorter duration compared with those on the ground. This is contrary to the expectation that the waveform in the ground experiment has a higher peak

and a shorter pulse width because the ambient pressure is much higher. In addition, there is a relationship between the peak value of the ESD current and the distance between ESD location and anode electrode. In order to investigate further, additional ESD experiments were conducted. Probes were added to measure the ESD current, the potential of experiment system, and the bias voltage. Thereby, small ESD currents which have a lower peak current than trigger level of HORYU-IV's measurement system can be measured. Furthermore, we added a video camera outside the chamber to take a picture of sparks of light from the ESD. Through the additional experiment, we found that the small ESDs which have less than 1 A of peak ESD current occurred at the distant location from anode electrode. This may be due to the effect of electric field around ESD location. It is considered that when ESD occurs at the distant location from the anode electrode, the emitted electron travels to the sheath boundary and then travels to the anode electrode. Since it is considered that the length of ESD current path and plasma resistance are proportional, the peak value of the ESD current may become smaller as the length of ESD route becomes longer. There are multiple other effects to determine the shape of the ESD current waveform, which is a subject for future investigation.

Acknowledgments

This research is supported by JSPS KAKENHI Grant Number 25220915S.

References

[1] Ferguson, D. C., "The Voltage Threshold for Arcing for Solar Cells in LEO-Flight and Ground Test Results," *24th Aerospace Sciences Meeting*, 1986.
doi: 10.2514/6.1986-362

[2] Lai, S. T., Dale C Ferguson, Hillard, G. B., Cho, M., Lai, S. T., Eliasson, L., Minow, J., and LiChao-jun, Z., *Spacecraft Charging*, 2011.

[3] Cho, M., Masui, H., Iwai, S., Yoke, T., and Toyoda, K., "Three Hundred Fifty Volt Photovoltaic Power Generation in Low Earth Orbit," *Journal of Spacecraft and Rockets*, vol. 51, 2014, pp. 379–381.
doi: 10.2514/1.A32559

[4] Yoke, T., Iwai, S., Khan, A. R., Masui, H., Iwata, M., Toyoda, K., and Cho, M., "Development of mission payloads onboard high voltage technology demonstration satellite HORYU-II," *IEEE Transactions on Plasma Science*, vol. 41, 2013, pp. 3477–3486.

doi: 10.1109/TPS.2013.2276439

[5] Iwai, S., Masui, H., Iwata, M., Toyoda, K., and Cho, M., “Flight Results of Arcing Experiment Onboard High-Voltage Technology Demonstration Satellite Horyu-2,” *Journal of Spacecraft and Rockets*, vol. 52, 2015, pp. 544–552.
doi: 10.2514/1.A33007

[6] Shimizu, T., Fukuda, H., Toyoda, K., and Cho, M., “Solar array electrostatic discharge current and image captured in orbit,” *Journal of Spacecraft and Rockets*, vol. 54, 2017, pp. 2–4.
doi: 10.2514/1.A33622

[7] Shimizu, T., Fukuda, H., Su, N. T., Toyoda, K., Iwata, M., and Cho, M., “Initial Results from an In-Orbit High-Voltage Experimental Platform: HORYU-IV,” *IEEE Transactions on Plasma Science*, vol. 45, 2017, pp. 1853–1863.
doi: 10.2514/1.A33007

[8] Shimizu, T., Fukuda, H., Toyoda, K., and Cho, M., “Development of an In-Orbit High-Voltage Experimental Platform: HORYU-4,” *IEEE Transactions on Plasma Science*, vol. 43, 2015, pp. 3027–3040.
doi: 10.1109/TPS.2015.2453330

[9] Okumura, T., Masui, H., Toyoda, K., Cho, M., Nitta, K., and Imaizumi, M., “Environmental Effects on Solar Array Electrostatic Discharge Current Waveforms and Test Results,” *Journal of Spacecraft and Rockets*, vol. 46, 2009, pp. 697–705.
doi: 10.2514/1.41696